Lattice determination of the QCD low-energy constant ℓ_7

Claudio Bonanno,[1,*] Gilberto Colangelo,[2,†] Francesco D'Angelo,[3,‡] Massimo D'Elia,[4,§] Roberto Dionisio,[4,‖] Roberto Frezzotti,[5,¶] Giuseppe Gagliardi,[6,**] Vittorio Lubicz,[6,††] Guido Martinelli,[7,‡‡] Francesco Sanfilippo,[3,§§] and Silvano Simula[3,‖‖]

[1]*Instituto de Física Teórica UAM-CSIC, c/ Nicolás Cabrera 13-15, Universidad Autónoma de Madrid, Cantoblanco, E-28049 Madrid, Spain*

[2]*Albert Einstein Center for Fundamental Physics, Institute for Theoretical Physics, University of Bern, Sidlerstrasse 5, 3012 Bern, Switzerland*

[3]*INFN, Sezione di Roma Tre, Via della Vasca Navale 84, I-00146 Rome, Italy*

[4]*Dipartimento di Fisica, Università di Pisa and INFN, Sezione di Pisa, Largo Pontecorvo 3, I-56127 Pisa, Italy*

[5]*Dipartimento di Fisica, Università di Roma "Tor Vergata" and INFN, Sezione di Roma Tor Vergata, Via della Ricerca Scientifica 1, I-00133 Rome, Italy*

[6]*Dipartimento di Matematica e Fisica, Università "Roma Tre" and INFN, Sezione di Roma Tre, Via della Vasca Navale 84, I-00146 Rome, Italy*

[7]*Dipartimento di Fisica, Università di Roma "La Sapienza" and INFN, Sezione di Roma La Sapienza, Piazzale Aldo Moro 5, I-00185 Rome, Italy*

(Received 17 December 2025; accepted 26 February 2026; published 15 April 2026)

We provide a nonperturbative determination of the scheme- and scale-independent low-energy constant ℓ_7, appearing in the QCD effective chiral Lagrangian at next-to-leading order, by means of lattice QCD simulations with $N_f = 2 + 1$ quark flavors. We adopt staggered fermions and extract ℓ_7 from the pion mass splitting by suitably generalizing the method introduced by Frezzotti *et al.* [Phys. Rev. D **104**, 074513 (2021)] for the Wilson discretization. Adopting 12 gauge ensembles with three different values of the pion mass, and four different values of the lattice spacing, we are able to achieve controlled extrapolations toward the continuum, infinite volume, and chiral limits. Our final result $\ell_7 \times 10^3 = 2.79(58)_{\text{stat}}(19)_{\text{syst}} = 2.79(61)_{\text{tot}}$ agrees with and substantially improves on previous determinations.

DOI: 10.1103/8sy5-f78d

I. INTRODUCTION

Effective field theories represent a powerful approach for studying quantum field theories in regimes where a full description across all energy scales is either impractical or unnecessary. They indeed provide a framework which allows one to capture the relevant dynamics at the desired energy scales through approximations that are, in principle, systematically improvable. In practice, effective theories are built as an expansion in one or more small quantities, and since the number of free parameters typically grows rapidly with the order of the expansion, this can potentially limit their applicability. However, there are many phenomenologically relevant cases where already the first few terms allow, in certain regimes, a satisfying approximation of very complex theories with a controllable number of parameters, the nonperturbative low-energy domain of quantum chromodynamics (QCD) being a paramount example.

In the limit of N_f massless quarks, the QCD Lagrangian exhibits a global $\mathrm{SU}(N_f)_L \times \mathrm{SU}(N_f)_R$ flavor symmetry, which is spontaneously broken to $\mathrm{SU}(N_f)_V$ at energy scales much smaller than Λ_{QCD} [1]. This fact allows a low-energy description of strong interactions by means of chiral perturbation theory (χPT), an effective theory describing massive QCD as a small perturbation around the chirally symmetric point with massless quarks.

The χPT Lagrangian is constructed by writing down all possible terms consistent with the symmetries of the theory

*Contact author: claudio.bonanno@csic.es
†Contact author: gilberto@itp.unibe.ch
‡Contact author: francesco.dangelo@roma3.infn.it
§Contact author: massimo.delia@unipi.it
‖Contact author: roberto.dionisio@phd.unipi.it
¶Contact author: roberto.frezzotti@roma2.infn.it
**Contact author: giuseppe.gagliardi@roma3.infn.it
††Contact author: vittorio.lubicz@uniroma3.it
‡‡Contact author: guido.martinelli@roma1.infn.it
§§Contact author: francesco.sanfilippo@roma3.infn.it
‖‖Contact author: simula@roma3.infn.it

in terms of the Nambu-Goldstone boson fields associated to chiral symmetry breaking, ordered in powers of the squared momenta p^2 and of the quark masses $m_{\rm q}$ (the so-called p expansion). Each order of this expansion introduces a set of parameters known as low energy constants (LECs), which encode the nonperturbative dynamics of the full theory, and must be fixed either phenomenologically from experimental data or through first-principles lattice QCD calculations. At leading order (LO) in p^2 and $m_{\rm q}$, the χPT Lagrangian contains only two LECs: the pion decay constant F and the quark condensate Σ. Instead, at next-to-leading order (NLO) $\mathcal{O}(p^4)$, and for $N_{\rm f}=2$ light quark flavors, one needs to introduce seven more LECs, $\{\ell_i\}_{i=1,\ldots,7}$. The value of all LECs depends on the strange quark mass $m_{\rm s}$.

Among them, the scheme and scale independent LEC ℓ_7 is the only one parametrizing strong isospin-breaking (IB) effects at NLO. For instance, it enters the strong charged/neutral pion mass splitting [2,3],

$$M^2_{\pi^+}-M^2_{\pi^0}=(\Delta m)^2\frac{8B^2}{F^2}\ell_7[1+\mathcal{O}(m_\ell)], \qquad (1)$$

where ($m_{\rm u}$, $m_{\rm d}$ are the up, down quark masses)

$$m_\ell\equiv\frac{1}{2}(m_{\rm d}+m_{\rm u}), \qquad \Delta m\equiv\frac{1}{2}(m_{\rm d}-m_{\rm u}), \qquad (2)$$

$B\equiv\Sigma/F^2$, and where we are adopting the convention $F_\pi^{(\rm phys)}\simeq 92$ MeV for physical quark masses. Thus, ℓ_7 plays a crucial role in several physical processes where IB effects are important, ranging from hadron physics to beyond standard model phenomenology. Despite its importance, among the seven $N_{\rm f}=2$ NLO χPT LECs, ℓ_7 is currently affected by the largest uncertainties, and the number of papers tackling its calculation is rather scarce. The first phenomenological estimate of ℓ_7 was given in [2,3] using arguments related to the $\eta-\pi_0$ mixing,

$$\ell_7=\frac{F_\pi^2}{6M_\eta^2}\sim 5\times 10^{-3}. \qquad (3)$$

However, NLO corrections turn out to be quite large and of the same order of LO contributions, thus giving rise to sizable systematics [4]: $\ell_7=7(4)\times 10^{-3}$.

On the other hand, also the current status of first-principles determination of ℓ_7 from numerical Monte Carlo simulations of lattice QCD is not very advanced (for a review on the status of the lattice determinations of the QCD LECs see Sec. 5 of Ref. [5]). The RBC-UKQCD Collaboration provided a first *indirect* determination of ℓ_7 in Ref. [6] through a global fit involving several pseudoscalar masses and decay constants: $\ell_7=6.5(3.8)\times 10^{-3}$. The accuracy of this determination is however comparable with the phenomenological estimate discussed above.

Improving the accuracy of current determinations of ℓ_7 has been recognized as a necessary ingredient for accurate predictions about axion physics. The axion mass m_a receives a NLO correction whose overall uncertainty is at the percent level, with the most significant contribution coming from the one on ℓ_7 [4,7]. Moreover, the dominant source of error in the determination of the axion quartic self-coupling λ_a (about 6%) comes from ℓ_7 too [4]. Finally, recent studies of axion-pion scattering within SU(2) χPT at NLO have shown that the error on ℓ_7 induces a 15%–20% uncertainty in the $a\pi\to\pi\pi$ amplitude, impacting constraints on the axion mass obtained from hot dark matter bounds [8–10].

Going beyond the present state of the art demands devising dedicated nonperturbative lattice strategies to effectively determine ℓ_7. Recently, progress in this direction has been achieved. More precisely, two *direct* lattice methods to compute ℓ_7 from lattice QCD have been proposed in Ref. [11], both rooted on the RM123 approach [12,13]. One is based on the calculation of the coupling between the neutral pion and the isosymmetric pseudoscalar quark density; the other, which is the one we will adopt in this study, is instead based on the calculation of the pion mass splitting in Eq. (1). The main idea behind this strategy is to evaluate the charged and neutral pion mass difference $M^2_{\pi^+}-M^2_{\pi^0}$ at order $\mathcal{O}[(\Delta m)^2]$ by expanding the path integral around the isosymmetric point $m_{\rm u}=m_{\rm d}\equiv m_\ell$ in powers of the quarks mass difference Δm. This makes it straightforward to directly evaluate derivatives of the pion mass difference with respect to Δm, which are indeed proportional to ℓ_7 itself, as we will discuss later. In the same paper [11], the authors also provided a proof-of-principle lattice calculation using rotated twisted mass fermions [14] for a single gauge ensemble, and were able to reduce the bound on ℓ_7 down to $\ell_7=2.5(1.4)\times 10^{-3}$ combining the results from the two methods.

Given the very promising results obtained in [11], in this work we aim at performing a dedicated lattice study targeting the determination of ℓ_7 using the same pion mass splitting method of [11], but implementing it with staggered fermions. This choice is motivated by the computational efficiency of the staggered discretization, which is significantly less expensive to simulate compared to other fermion formulations; moreover, checking the consistency of determinations obtained adopting different fermion discretizations represents, as usual, a solid test of universality and of the claimed control over the systematic effects which may affect lattice QCD results.

Clearly, staggered fermions also present additional complications related to the breaking of taste symmetry at finite lattice spacing which require particular attention. Despite these challenges, we were able to generalize the strategy of [11] to staggered quarks, and apply it to several staggered gauge ensembles obtaining reliable results for ℓ_7. This allowed us to obtain controlled continuum and chiral

extrapolations of this quantity for the first time, and to attain an overall final uncertainty which significantly improves on previous estimates.

This paper is organized as follows: in Sec. II we describe our numerical setup and the mass-splitting method we adopted to compute ℓ_7; in Sec. III we present our results for ℓ_7; finally, in Sec. IV we draw our conclusions.

II. NUMERICAL SETUP

A. Lattice QCD discretization and simulation parameters

The numerical setup (i.e., the lattice QCD discretization and the algorithm employed for the Monte Carlo sampling of the path integral) and the gauge ensembles adopted here are both inherited from the previous study [15].

We discretize QCD on an hypercubic N_s^4 space-time lattice, with periodic (antiperiodic) boundary conditions for gluons (quarks). We adopt a tree-level Symanzik-improved action for the gluonic sector,

$$S_{\rm YM}^{(\rm L)}[U] = -\frac{\beta}{3}\sum_{x,\mu\neq\nu}\left\{\frac{5}{6}\Re{\rm Tr}\left[\Pi_{\mu\nu}^{(1\times1)}(x)\right] + -\frac{1}{12}\Re{\rm Tr}\left[\Pi_{\mu\nu}^{(1\times2)}(x)\right]\right\}, \tag{4}$$

with $\Pi_{\mu\nu}^{(n\times m)}(x)$ being the product of gauge links along $n\times m$ rectangular paths starting at point x and extending in the (μ,ν) plane. The fermionic sector consists of $N_{\rm f}=2+1$ flavors of rooted stout-smeared staggered fermions. The fermion matrix is given by,

$$\mathcal{M}_{\rm f}^{(\rm stag)}[U] \equiv D_{\rm stag}[U^{(2)}] + am_{\rm f}, \tag{5}$$

$$D_{\rm stag}[U^{(2)}] = \sum_{\mu=1}^{4}\eta_\mu(x)[U_\mu^{(2)}(x)\delta_{x,y-\hat\mu} - U_\mu^{(2)\,\dagger}(x-\hat\mu)\delta_{x,y+\hat\mu}], \tag{6}$$

$$\eta_\mu(x) = (-1)^{x_1+\cdots+x_{\mu-1}}, \tag{7}$$

with $\eta_\mu(x)$ the so called staggered phases, a the lattice spacing, $m_{\rm f}$ the bare mass of the quark flavor f, and where the stouted links $U_\mu^{(2)}(x)$ are taken after two steps of isotropic stout smearing with $\rho_{\rm stout}=0.15$ [16].

The total partition function,

$$Z_{\rm LQCD} = \int [{\rm d}U]{\rm e}^{-S_{\rm YM}^{(\rm L)}[U]}\times\det\{\mathcal{M}_\ell^{(\rm stag)}[U]\}^{\frac{1}{2}} \times\det\{\mathcal{M}_{\rm s}^{(\rm stag)}[U]\}^{\frac{1}{4}}, \tag{8}$$

with ℓ and s labeling the light and strange quark flavors, respectively, has been sampled with the rational hybrid Monte Carlo (RHMC) algorithm [17,18].

In this work we will employ 12 different gauge ensembles, whose simulation parameters are reported in Table I. These ensembles correspond to three different lines of constant physics (LCPs) where the lattice size is fixed to $L\equiv aN_{\rm s}\simeq 3$ fm, the bare strange quark mass $m_{\rm s}$ is tuned to keep its renormalized value constant and equal to its physical value $m_{\rm s}^{(\rm phys)}$, and the bare mass of the degenerate light doublet $m_{\rm u}=m_{\rm d}=m_\ell$ is varied to explore different values of the pion mass M_π. These LCPs were determined in Ref. [15], starting from the results of Refs. [19–21] for the bare parameters belonging to the physical point LCP, by varying the bare light quark mass at fixed bare strange quark mass. More precisely, we considered light-to-strange quark mass ratios $R\equiv m_\ell/m_{\rm s}^{(\rm phys)}$ equal to 4, 6 and 9 times the physical ratio $R^{(\rm phys)}=m_\ell^{(\rm phys)}/m_{\rm s}^{(\rm phys)}$ determined in Refs. [19–21]. These choices correspond to $M_\pi^2\simeq 4,6,9M_\pi^{(\rm phys)2}$, $M_\pi^{(\rm phys)}=135$ MeV, and $M_\pi L\geq 4$, a value that is sufficient to keep finite-size effects below our statistical errors, as we shall discuss later. For each LCP we considered four values of the lattice spacing a ranging from ∼0.15 fm to ∼0.075 fm. Our setup thus allows us to take continuum limits $a\to 0$ at fixed light and strange quark masses, and then to take the SU(2) chiral limit $m_\ell\to 0$ at fixed physical strange quark mass $m_{\rm s}^{(\rm phys)}$, i.e., $R\to 0$. Further details about the determination of the LCP simulation parameters can be found in the original paper [15].[1]

B. ℓ_7 from the mass-splitting method

The mass-splitting method of [11] relies on two main ingredients: the fact that the strong charged/neutral pion mass difference induced by strong IB effects is parametrized by ℓ_7 via Eq. (1); and the fact that this formula can be directly evaluated at the first nontrivial order in Δm by using the RM123 method.

The starting point is to rewrite (1) in a way that is more suitable for a numerical evaluation. By expanding the left-hand side at LO in Δm and using the χPT LO relation $M^2=B(m_{\rm u}+m_{\rm d})=2Bm_\ell$, we have,

$$M_{\pi^+}^2 - M_{\pi^0}^2 \simeq 2M(M_{\pi^+}-M_{\pi^0}) = (\Delta m)^2\frac{2M^4}{m_\ell^2F^2}\ell_7, \tag{9}$$

[1]The results for F_π in Table I correct those originally given in Ref. [15], whose calculation was affected by a mismatch in the renormalization constants, resulting in a ∼15%–19% shift upward. This issue regarded the analysis of the ensembles at heavier than physical pions, and it does not affect the chiral limit of F_π given in [15], but only its slope as a function of M_π. The latter was not discussed in [15], and it is reported for the first time in the present work in Appendix E.

TABLE I. Summary of the simulation parameters of the gauge ensembles employed in this study. The LCP parameters, including pion masses and lattice spacings, were obtained in [15] starting from the physical point LCP determined in [19–21]. The values of the lattice spacing have been determined in [15] with the w_0 scale setting approach [22] with a ∼2% error at most, and their value in fm units was obtained assuming $w_0 = 0.1757(12)$ fm [22] for all ensembles, independently of the pion mass. The variable $N_{\rm conf}$ is the number of thermalized gauge configurations generated for each ensemble, each separated by 10 RHMC updating steps. For each ensemble we also report the values of M_π and F_π.

$R \equiv m_\ell/m_{\rm s}^{(\rm phys)}$	β	$N_{\rm s}$	am_ℓ	$am_{\rm s}$	a (fm)	$N_{\rm conf}$	M_π (MeV)	F_π (MeV)	$L = aN_{\rm s}$ (fm)	$M_\pi L$
0.1421	3.67838	20	0.008828	0.062136	0.1515	6200	260(3)	98.5(2.1)	3.03	4.00
	3.75000	24	0.007150	0.050300	0.1265	5400	262(3)	99.0(2.3)	3.04	4.08
	3.86847	32	0.005383	0.037884	0.0964	3373	263(4)	98.9(2.2)	3.08	4.21
	3.98775	40	0.004244	0.029867	0.0758	3160	269(5)	98.4(2.3)	3.03	4.13
0.2131	3.67838	20	0.013242	0.062136	0.1532	1800	320(2)	102.4(2.7)	3.06	4.96
	3.75000	24	0.010722	0.050300	0.1278	1800	315(3)	101.8(2.5)	3.07	4.90
	3.86847	32	0.008075	0.037884	0.0976	2730	315(5)	100.9(2.4)	3.12	4.98
	3.98775	40	0.006366	0.029867	0.0764	1390	317(6)	101.1(2.5)	3.06	4.92
0.3197	3.67838	20	0.019863	0.062136	0.1556	1320	381(1)	106.8(2.6)	3.11	6.00
	3.75000	24	0.016080	0.050300	0.1297	1280	382(2)	105.8(2.4)	3.11	6.02
	3.86847	32	0.012112	0.037884	0.0989	1250	380(1)	105.5(2.5)	3.16	6.09
	3.98775	40	0.009549	0.029867	0.0768	1320	386(4)	106.3(2.6)	3.07	6.01

$$\Rightarrow \ell_7 = \frac{m_\ell^2 F^2}{M^3} \times \frac{(M_{\pi^+} - M_{\pi^0})_{\rm QCD}}{(\Delta m)^2}, \tag{10}$$

where $(M_{\pi^+} - M_{\pi^0})_{\rm QCD}$ denotes the mass splitting arising solely from the up/down quark mass difference, i.e., excluding $\mathcal{O}(\alpha_{\rm em})$ electromagnetic effects. Thus, at the order in Δm at which we are working, the computation of ℓ_7 is reduced to the computation of,

$$\frac{(M_{\pi^+} - M_{\pi^0})_{\rm QCD}}{(\Delta m)^2} = \frac{1}{2}(M''_{\pi^+} - M''_{\pi^0})_{\rm isoQCD} + \mathcal{O}(\Delta m) \tag{11}$$

in isosymmetric QCD (i.e., the theory with $\Delta m = 0$), with $'$ denoting differentiation with respect to Δm.

Such a quantity can be extracted on the lattice from the second derivative with respect to Δm of the difference $C_{\pi^+\pi^+}(t) - C_{\pi^0\pi^0}(t)$ between the Euclidean time correlation functions of the charged and neutral pions. As a matter of fact, the asymptotic behavior of these correlators for large Euclidean time separations is,

$$\begin{aligned} C_{\pi^+\pi^+}(t) &\underset{a\ll t\ll T}{\sim} A_{\pi^+} \cosh\left[M_{\pi^+}\left(\frac{T}{2} - t\right)\right], \\ C_{\pi^0\pi^0}(t) &\underset{a\ll t\ll T}{\sim} A_{\pi^0} \cosh\left[M_{\pi^0}\left(\frac{T}{2} - t\right)\right], \end{aligned} \tag{12}$$

where $T = aN_{\rm s}$ is the Euclidean time extent of the lattice, and $A_{\rm P}$ represents the amplitude for the particle P obtained from the interpolating operator $\mathcal{O}_{\rm P}$,

$$A_{\rm P} = \frac{|Z_{\rm PP}|^2}{M_{\rm P}} {\rm e}^{-M_{\rm P}\frac{T}{2}}, \tag{13}$$

$$Z_{\rm PP} = \langle {\rm P}|\mathcal{O}_{\rm P}|0\rangle. \tag{14}$$

Therefore, by taking derivatives with respect to Δm one obtains [11],

$$\begin{aligned} &\frac{[C''_{\pi^+\pi^+}(t) - C''_{\pi^0\pi^0}(t)]_{\rm isoQCD}}{C_{\pi\pi}^{(\rm isoQCD)}(t)} \underset{a\ll t\ll T}{\sim} \\ &\frac{A''_{\pi^+} - A''_{\pi^0}}{A_\pi} + (M''_{\pi^+} - M''_{\pi^0})\left(\frac{T}{2} - t\right) \\ &\times \tanh\left[M_\pi\left(\frac{T}{2} - t\right)\right] a \end{aligned} \tag{15}$$

with $C_{\pi\pi}^{(\rm isoQCD)}(t)$ the usual pion correlator computed in isosymmetric QCD.

To obtain the numerator of the left-hand side of Eq. (15) from an actual lattice QCD Monte Carlo calculation and extract $(M''_{\pi^+} - M''_{\pi^0})$, we follow the RM123 approach [12], which allows one to evaluate derivatives with respect to Δm by expanding around isoQCD. Let us briefly introduce this method by starting from the fermionic part of the Euclidean QCD Lagrangian for a nondegenerate light quark doublet $\psi = (\psi_{\rm u}, \psi_{\rm d})$,

$$\mathcal{L}_{\rm q} = \bar\psi(\gamma_\mu D_\mu + \mathcal{M})\psi, \tag{16}$$

where $\mathcal{M}$ is the mass matrix, diagonal in flavor space, i.e., $\mathcal{M} = {\rm diag}(m_{\rm u}, m_{\rm d})$. The mass term can be written as a sum of a SU(2) symmetric part and a term which explicitly breaks the isospin symmetry,

$$\begin{aligned}\mathcal{L}_m &= \frac{m_u + m_d}{2}(\bar{\psi}_u\psi_u + \bar{\psi}_d\psi_d) \\ &\quad - \frac{m_d - m_u}{2}(\bar{\psi}_u\psi_u - \bar{\psi}_d\psi_d) \\ &= m_\ell(\bar{\psi}_u\psi_u + \bar{\psi}_d\psi_d) - \Delta m(\bar{\psi}_u\psi_u - \bar{\psi}_d\psi_d) \\ &= m_\ell\bar{\psi}\psi - \Delta m\bar{\psi}\tau_3\psi, \end{aligned} \tag{17}$$

with $\tau_3 = \mathrm{diag}(1,-1)$ being the third Pauli matrix. This allows us to isolate the IB contribution $\mathcal{L}_{IB}$ within the starting Lagrangian (16) as,

$$\mathcal{L}_q = \underbrace{\bar{\psi}(\gamma_\mu D_\mu + m_\ell)\psi}_{\mathcal{L}_0} - \underbrace{\Delta m\bar{\psi}\tau_3\psi}_{\mathcal{L}_{IB}}. \tag{18}$$

Within the RM123 approach, $\mathcal{L}_{IB}$ is treated as a perturbation with respect to $\mathcal{L}_0$, and the path integral is expanded around the isosymmetric point $m_u = m_d \equiv m_\ell$. The vacuum expectation value (VEV) of a generic observable $\mathcal{O}$ can then be computed as follows:

$$\begin{aligned}\langle\mathcal{O}\rangle &= \langle\mathcal{O}\rangle_0 - \underbrace{\langle\mathcal{O}S_{IB}\rangle_0}_{\mathcal{O}(\Delta m)} \\ &\quad + \underbrace{\frac{1}{2}[\langle\mathcal{O}S_{IB}^2\rangle_0 - \langle\mathcal{O}\rangle_0\langle S_{IB}^2\rangle_0]}_{\mathcal{O}[(\Delta m)^2]} \\ &\quad + \mathcal{O}[(\Delta m)^3], \end{aligned} \tag{19}$$

where $\langle\ldots\rangle_0$ represents the VEV with respect to the isosymmetric theory (recall that $\langle S_{IB}\rangle_0 = \langle\int d^4x\mathcal{L}_{IB}\rangle_0 = 0$).

Using the RM123 approach outlined so far, one can expand the difference between the charged/neutral pion correlators in powers of Δm. Performing the relevant Wick contractions, one obtains the following diagrammatic expansion at the first nontrivial order [11],

$$\begin{aligned}&C_{\pi^+\pi^+}(t) - C_{\pi^0\pi^0}(t) = \\ &= 2\,(Z_S Z_m)^2\,(\Delta m)^2 \\ &\quad \times \Big[\quad - \quad \Big] \\ &\equiv 2\,(Z_S Z_m)^2\,(\Delta m)^2\left[C_{4pt}^{(conn)}(t) - C_{4pt}^{(disc)}(t)\right] \\ &= 2(\Delta m)^2\left[C_{4pt}^{(conn)}(t) - C_{4pt}^{(disc)}(t)\right], \end{aligned} \tag{20}$$

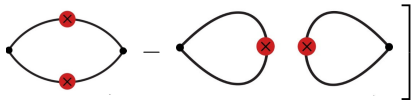

where we have denoted with $C_{4pt}^{(conn)}(t)$ and $C_{4pt}^{(disc)}(t)$, respectively, the connected and disconnected four-point correlation functions arising at $\mathcal{O}[(\Delta m)^2]$ in the RM123 expansion of $C_{\pi^+\pi^+}(t) - C_{\pi^0\pi^0}(t)$.

In the diagrammatic representation of these 4-point correlators, the full dots in the previous diagrams denote an insertion of γ_5, while the crossed ones correspond to an insertion of $S_{IB} = \int d^4x\mathcal{L}_{IB}$. We also included the renormalization constants for the mass and for the scalar density Z_m, Z_S due, respectively, to the factors of Δm and $\bar{\psi}\tau_3\psi$ in $\mathcal{L}_{IB}$. However, within our staggered fermion discretization, $Z_m = Z_S^{-1}$, thus the quantity in (20) is a renormalization group invariant [23].

Given that, at the first nontrivial order in Δm,

$$\begin{aligned}C_{\pi^+\pi^+}(t) - C_{\pi^0\pi^0}(t) &= \frac{(\Delta m)^2}{2} \\ &\quad \times [C''_{\pi^+\pi^+}(t) - C''_{\pi^0\pi^0}(t)]_{\Delta m=0}, \end{aligned} \tag{21}$$

we recognize that,

$$\begin{aligned}&\frac{1}{2}[C''_{\pi^+\pi^+}(t) - C''_{\pi^0\pi^0}(t)]_{\Delta m=0} \\ &\quad = 2[C_{4pt}^{(conn)}(t) - C_{4pt}^{(disc)}(t)]. \end{aligned} \tag{22}$$

In the end, we can construct the following lattice estimator for ℓ_7:

$$\begin{aligned}\ell_7^{(eff)}(t) &\equiv \frac{2F_\pi^2 m_\ell^2}{M_\pi^3}\frac{1}{\mathcal{F}(\frac{T}{2} - t, M_\pi)}\left[\frac{\delta C}{C}(t) - \frac{\delta C}{C}(t-a)\right], \\ \frac{\delta C}{C}(t) &\equiv \frac{[C_{4pt}^{(conn)}(t) - C_{4pt}^{(disc)}(t)]_{isoQCD}}{C_{\pi\pi}^{(isoQCD)}(t)}, \\ \mathcal{F}(x,M) &\equiv x\,\tanh\,(Mx) - (x+a)\tanh\,[M(x+a)], \end{aligned} \tag{23}$$

with a the lattice spacing, and M_π, F_π the finite-quark-mass determinations of these quantities in Table I. The function $\ell_7^{(eff)}(t)$, for asymptotically large time separations, will tend to ℓ_7.

Finally, on the technical side, both the 2-point and the 4-point correlators entering the estimator (23) were computed using standard stochastic methods, using temporal dilution with one stochastic source per time slice in order to invert the staggered Dirac operator. We also verified in a few cases that increasing the number of sources gave compatible error estimates.

III. NUMERICAL RESULTS

A. Lattice determination of ℓ_7

In this section we will exemplify the lattice determination of ℓ_7 from the mass-splitting method introduced in Sec. II B for one gauge ensemble.

Let us start by discussing the evaluation of the correlation functions entering the ℓ_7 estimator in Eq. (23). As it is well known, see, e.g., Refs. [20,24,25], when using staggered fermions there are several choices for the pion interpolating operator,

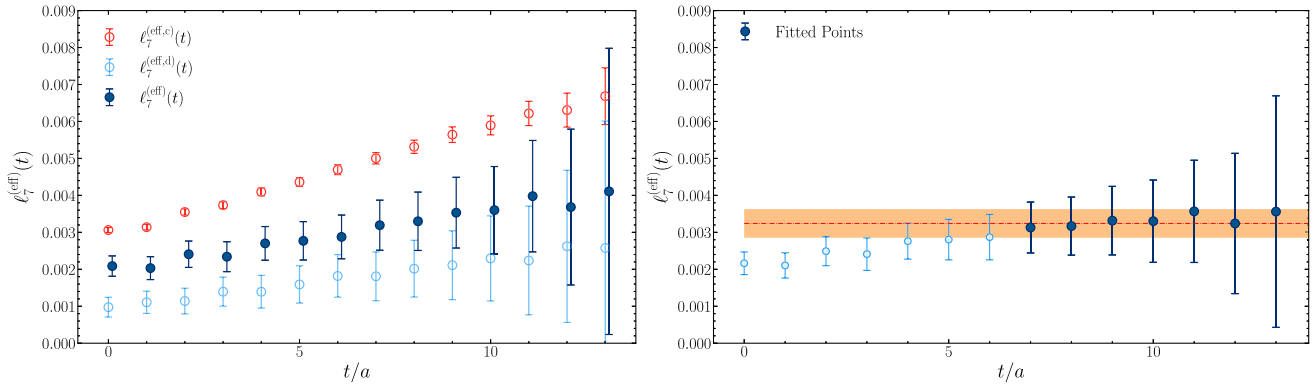

FIG. 1. Left panel: lattice estimator $\ell_7^{(\mathrm{eff})}(t)$ and individual contributions of the connected/disconnected diagrams to this function for the ensemble with $R \simeq 0.1421$ and $a = 0.0964$ fm. Right panel: extraction of ℓ_7 from the large-time-separation plateau exhibited by $\ell_7^{(\mathrm{eff})}(t)$.

$$\mathcal{O}_\pi^{(\mathrm{S})} = \bar{\psi}\gamma_5 \otimes \xi_{\mathrm{S}}\psi, \tag{24}$$

each one corresponding to a different spin-taste structure: $\mathrm{S} = (\mathrm{I}, \mathrm{P}, \mathrm{V}, \mathrm{A}, \mathrm{T})$, labeling, respectively, the scalar, pseudoscalar, vector, axial-vector and tensor channels. Due to explicit taste breaking at finite lattice spacing, the ground state masses in each of these channels differ among themselves, but they all converge to the same value in the continuum limit (see Appendix A more details on this point). However, at finite lattice spacing, only the pseudoscalar channel, $\xi_{\mathrm{P}} = \xi_5$, corresponds to an actual pseudo-Nambu–Goldstone boson whose mass is protected by the remnant of the continuum chiral symmetry enjoyed by staggered fermions. Thus, this is customarily the preferred choice for the pion interpolating operator in most lattice calculations involving the staggered discretization. As a matter of fact, for the isoQCD 2-point pion correlation function and the extraction of M_π and F_π, whose calculation was tackled in the previous study [15], and to which we refer for more details, this was indeed the case.

Instead, concerning the 4-point correlators $C_{4\mathrm{pt}}^{(\mathrm{conn})}$ and $C_{4\mathrm{pt}}^{(\mathrm{disc})}$, we found that the standard pseudoscalar channel was revealed to be impractical, as with this choice of the pion interpolating operator the disconnected correlator turned out to be completely dominated by statistical noise, and remained compatible with zero within errors for all time separations.[2] Thus, the pseudoscalar channel does not allow for a reliable extraction of ℓ_7, motivating the need to explore alternative spin-taste structures. The first natural candidate beyond the pseudoscalar channel is the axial-vector one, corresponding to $\xi_{\mathrm{A}} = \xi_{5\mu}$. In this case, both the connected and disconnected diagrams exhibit nonzero signal with reasonable statistical quality, thus allowing a reliable calculation of the estimator $\ell_7^{(\mathrm{eff})}(t)$ (see Appendix B for a comparison of the obtained results for the disconnected contribution to ℓ_7 from the pseudoscalar and the axial channels). As a further check, we also verified that compatible results for ℓ_7 are obtained from the vector channel ($\xi_{\mathrm{V}} = \xi_\mu$) once the continuum limit is taken, although within larger error bars, see Appendix B, thus motivating our choice of the axial-vector channel.

In Fig. 1 (left panel), we show the time-dependence of the estimator $\ell_7^{(\mathrm{eff})}(t)$ for the ensemble with $m_\ell = 4m_\ell^{(\mathrm{phys})}$ and lattice spacing $a \simeq 0.0964$ fm. In order to illustrate how the physical signal for ℓ_7 arises from the difference of the connected and disconnected correlation functions of Eq. (20), we also plotted in the same figure the individual contributions to $\ell_7^{(\mathrm{eff})}(t)$ of the connected (c) and disconnected (d) diagrams, which are such that,

$$\ell_7^{(\mathrm{eff})}(t) = \ell_7^{(\mathrm{eff,c})}(t) - \ell_7^{(\mathrm{eff,d})}(t). \tag{25}$$

As it can be appreciated from Fig. 1 (right panel), the estimator exhibits a plateau for large time separations.

More precisely, for the case at hand, we observe the onset of the plateau for $t \geq 8a = T/4$. It is reassuring to find the onset of the plateau for F_π and M_π in similar time ranges, cf. for example Fig. 6 in Ref. [15]. The evaluation of ℓ_7 is thus performed via a constant best fit in a region close to $T/2$, where contamination of excited states is minimized, and the ground-state dominance is expected. The time window for the best fit was chosen by ensuring stability of the central value upon variation of the lower/upper range, and reasonable reduced χ^2, while the final error was assessed via a binned bootstrap analysis; typical windows are $[t_{\mathrm{min}}, t_{\mathrm{max}}]$ with $t_{\mathrm{min}}/T \sim 0.2 - 0.3$ and $t_{\mathrm{max}}/T \sim 0.4 - 0.45$.

[2]A similar behavior for disconnected diagrams in the pseudoscalar channel was observed in Ref. [26]. In that study it is pointed out that a term appearing in the effective staggered χPT Lagrangian allows disconnected contributions in the meson propagator only in the singlet, vector, and axial vector channels. Thus, to study the η and η' mesons, where disconnected diagrams are crucial due to their flavor-singlet nature, the $\gamma_5 \times \mathrm{I}$ interpolating operator was employed, as it is the only pseudoscalar bilinear with a nonvanishing disconnected contribution in the staggered case.

TABLE II. Summary of all direct lattice determinations of ℓ_7 as a function of a and of the parameter R (proportional to the light quark masses m_ℓ) using the mass-splitting method. We also report the squared pion mass splitting $\Delta \equiv M_\pi^2(\xi_A) - M_\pi^2(\xi_P)$ between the axial-vector and the pseudoscalar channel in units of $1/w_0^2$, which will be used for the study of systematic errors, see Sec. III C. The error on $w_0^2\Delta$ is of the order of ∼2% at most.

$R \equiv m_\ell/m_s^{(\mathrm{phys})}$	a [fm]	$\ell_7 \times 10^3$	$w_0^2\Delta$
0.1421	0.1515	1.11(37)	0.0587
	0.1265	2.18(25)	0.0400
	0.0964	3.25(38)	0.0203
	0.0758	3.67(40)	0.00990
0.2131	0.1532	3.18(89)	0.0611
	0.1278	3.56(48)	0.0409
	0.0976	4.36(43)	0.0208
	0.0764	4.62(38)	0.00994
0.3197	0.1556	4.73(88)	0.0648
	0.1297	5.16(57)	0.0433
	0.0989	6.21(51)	0.0215
	0.0768	6.08(36)	0.0101

The obtained values of ℓ_7 for all ensembles are collected in Table II.

We conclude by reporting for comparison the result from the mass splitting method obtained in Ref. [11] with twisted mass Wilson fermions, for a lattice spacing $a \simeq 0.095$ fm, a pion mass $M_\pi \simeq 260$ MeV, and a volume $M_\pi L \simeq 4$,

$$\ell_7 \times 10^3 = 3.5(2.0), \qquad (\text{Ref. } [11]). \tag{26}$$

Among our ensembles we have one with the same values of the lattice spacing, of the pion mass and of the lattice volume, namely, our next-to-finest lattice spacing ensemble for the smallest value of R simulated, cf. Table I. With staggered fermions in this case we find:

$$\ell_7 \times 10^3 = 3.25(38), \qquad (\text{this study}). \tag{27}$$

It should be noted that the error reduction achieved here cannot be entirely ascribed to the different sample sizes, as our statistics is larger by about a factor of 3 with respect to the one of [11], but we find a smaller uncertainty by about a factor of 5.[3]

[3]On the other hand, the statistical accuracies of F_π and M_π obtained with staggered quarks here and with twisted mass Wilson fermions in [11] are similar. More comprehensive investigations with other discretizations and possibly with mixed action setups are needed to clarify how the statistical accuracies of different types of observables depend on the chosen fermion formulation.

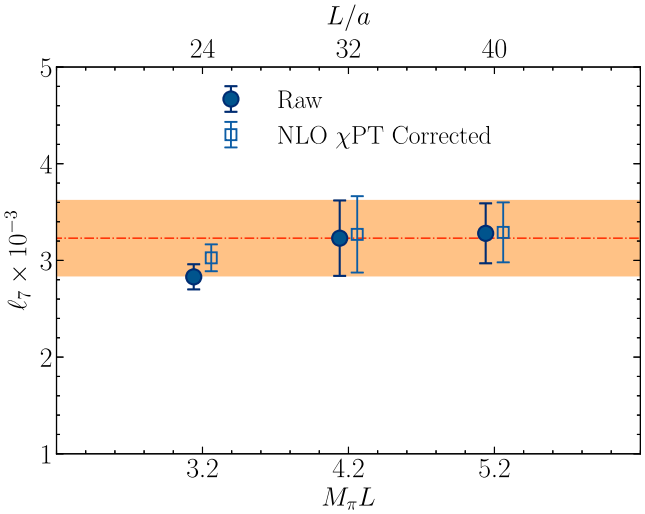

FIG. 2. Study of finite-size effects on ℓ_7 for our ensemble with $a = 0.0964$ fm and $M_\pi = 263(4)$ MeV. They are invisible within our statistical errors for $M_\pi L \geq 4$. The same conclusions are reached after subtracting finite-size effects estimated from NLO χPT: $\ell_7(L) \to \ell_7(L)/[1 + R_{\ell_7}(L)]$, see Sec. III B.

B. Finite-size effects on ℓ_7

Concerning finite-size effects, as outlined in Sec. II, we chose for all our simulations a lattice size of $L = aN_s \simeq 3$ fm, corresponding to $M_\pi L \simeq 4$, 5, 6 for the three sets of ensembles with $M_\pi \simeq 265$, 316, 384 MeV we considered.

For the next-to-finest lattice spacing of our lightest ensembles with $M_\pi L \simeq 4$ we explicitly checked that this threshold is sufficient to keep finite-size effects under control by performing two additional simulations for a smaller and a larger value of $M_\pi L \simeq 3$ and 5. The results of this test, shown in Fig. 2, indeed confirm that our choice for the lattice volume is safe. Such conclusion is also supported by analytical results obtained from NLO χPT. Indeed, analytic expressions for the volume-dependence of M_π and F_π are available up to NLO in the chiral expansion [27,28] (for the pion mass, also next-to-next-to-leading-order (NNLO) effects are known [29] and have been included in our calculation),

$$M_\pi(L) = M_\pi[1 + R_{M_\pi}(L)], \tag{28}$$

$$F_\pi(L) = F_\pi[1 + R_{F_\pi}(L)], \tag{29}$$

$$\Rightarrow \ell_7(L) = \ell_7\{1 + 2[R_{F_\pi}(L) - R_{M_\pi}(L)]\}, \tag{30}$$

with R_{M_π} and R_{F_π} given by Eqs. (26) and (27) of [28].

We find that $R_{\ell_7}(L) \equiv 2[R_{F_\pi}(L) - R_{M_\pi}(L)]$ is about $R_{\ell_7}(L) \simeq -6.5\%, -1.2\%, -0.3\%$ for $M_\pi L \simeq 3$, 4, 5, cf. Fig. 2. Based on the difference between NLO and NNLO results for R_{M_π}, we estimate that the reported numbers for R_{ℓ_7} are affected by at most a ∼1% error

due to the truncation of the chiral expansion. Since finite-volume effects estimated from $R_{\ell_7}(L)$ are at least one order of magnitude smaller than our statistical errors on ℓ_7 for $M_\pi L \geq 4$, we conclude that they are completely negligible with our current precision.

C. Continuum extrapolations of ℓ_7

After the extraction of ℓ_7 at finite lattice spacing and quark mass, we have all the necessary ingredients to perform continuum and chiral extrapolations.

Let us start from the continuum limit, which is taken in all cases at fixed value of the light and strange quark mass, i.e., at fixed value of $R = m_\ell/m_{\rm s}^{(\rm phys)}$. The continuum extrapolations were carried out by fitting our data with a few *Ansätze*:

$$\ell_7(a^2,R) = \ell_7(R) + C_2(R)a^2, \qquad \text{(A1)},$$
$$\ell_7(a^2,R) = \ell_7(R) + C_2(R)a^2 + C_4(R)a^4, \qquad \text{(A2)},$$
$$\ell_7(\Delta,R) = \ell_7(R) + C_2'(R)w_0^2\Delta, \qquad \text{(A3)},$$
$$\ell_7(\Delta,R) = \ell_7(R) + C_2'(R)w_0^2\Delta + C_4'(R)w_0^4\Delta^2, \qquad \text{(A4)},$$

where for the fit *Ansätze* A1 and A3 we performed two fits excluding/including the coarsest lattice spacing. In all formulas, $\ell_7(R)$ denotes the continuum-extrapolated value, while Δ denotes the taste-splitting between the squared axial-vector and pseudoscalar pion masses,

$$\Delta \equiv M_\pi^2(\xi_{\rm A}) - M_\pi^2(\xi_{\rm P}), \tag{31}$$

whose values in units of $1/w_0$ are reported in Table II. The fit *Ansätze* A3 and A4 are rooted on Symanzik effective theory (SYMEFT), which predicts that leading-order a^2 lattice artifacts are modified as $a^2\alpha_{\rm s}^n(\mu = 1/a)$ [30,31], with $\alpha_{\rm s}(\mu)$ the running strong coupling, and n depending on the particular sea and valence discretizations considered. Our choice of the quantity $w_0^2\Delta$ follows the proposal of Ref. [32] [cf. Eqs. (17) and (18) in Sec. IV of that study], where the authors study hadronic contributions to the anomalous muon magnetic moment with stout-smeared rooted staggered fermions. In particular, the authors observe that Δ vanishes approaching the continuum limit with a rate which is approximately $\Delta(a) \underset{a\to 0}{\sim} a^2\alpha_{\rm s}^3(\mu = 1/a)$, and thus use this quantity in their SYMEFT-inspired fit *Ansätze* to study systematic errors related to the continuum limit.

As it can be appreciated from Fig. 3, our data can be nicely fitted with $\mathcal{O}(a^2)$ corrections both when including/excluding the data at the coarsest lattice spacing, all giving perfectly compatible results within errors. Similar conclusions are drawn including a further a^4 term, or adopting the fit *Ansätze* based on SYMEFT.

Given the overall good agreement among all possible continuum limit fit functions, in all cases we considered the outcome of the linear fit in a^2, performed considering all lattice spacings, to assign a central value and a statistical error to our continuum determinations of $\ell_7(R)$. In addition to statistical uncertainties, we also assigned to our continuum extrapolations a systematic error related to the small difference observed when extrapolating our data with different fit *Ansätze*. Following the procedure outlined in [15,33], we computed,

$$\Delta_{\rm A} = \frac{|[\ell_7(R)]_{\rm A1} - [\ell_7(R)]_{\rm A}|}{\sqrt{\Delta^2_{\rm stat}[\ell_7(R)]_{\rm A1} + \Delta^2_{\rm stat}[\ell_7(R)]_{\rm A}}}, \tag{32}$$

which quantifies the relative difference between the central values obtained with the fit *Ansatz* A1 (including all lattice spacings) and another fit *Ansatz* "A" among the ones earlier listed.

The systematic error was then estimated as,

$$\Delta_{\rm syst,A} = |[\ell_7(R)]_{\rm A1} - [\ell_7(R)]_{\rm A}|\,{\rm erf}\left(\frac{\Delta_{\rm A}}{\sqrt{2}}\right), \tag{33}$$

where $\mathrm{erf}(x)$ denotes the standard error function,

$$\mathrm{erf}(x) = \frac{2}{\sqrt{\pi}}\int_0^x {\rm d}t\, {\rm e}^{-t^2}. \tag{34}$$

The quantity (33) represents the mismatch between the central values of the two fit *Ansätze*, weighted with an estimation of the probability that this mismatch is not due to a statistical fluctuation. All sources of systematic errors are then summed in quadrature: $\Delta_{\rm syst} = \sqrt{\sum_{\rm A}\Delta_{\rm A}^2}$. The final continuum extrapolations for each value of R, including systematic errors, are collected in Table III. As it can be appreciated, systematic errors are always subdominant with respect to statistical errors: even for $R \simeq 0.1421$, which has the largest systematic error, the statistical error is still ∼85% of the total budget (computed as the quadrature sum of the two uncertainties).

D. Chiral extrapolation of ℓ_7

We are now ready to extrapolate our continuum results at finite quark mass toward the SU(2) chiral limit, $m_\ell \to 0$ at fixed $m_{\rm s} = m_{\rm s}^{(\rm phys)}$, which in our setup corresponds to $R = m_\ell/m_{\rm s}^{(\rm phys)} \to 0$.

To achieve a solid control on the chiral extrapolation, it is fundamental to know the analytic form of the leading finite-quark mass contributions to ℓ_7. This in turn requires the knowledge of the NNLO contributions to the pion mass splitting in χPT. Despite the proliferation of operators entering the effective Lagrangian at this order of the chiral expansion, there are only a few isospin-breaking operators at $\mathcal{O}(p^6)$ [34]. This makes it feasible to work out the

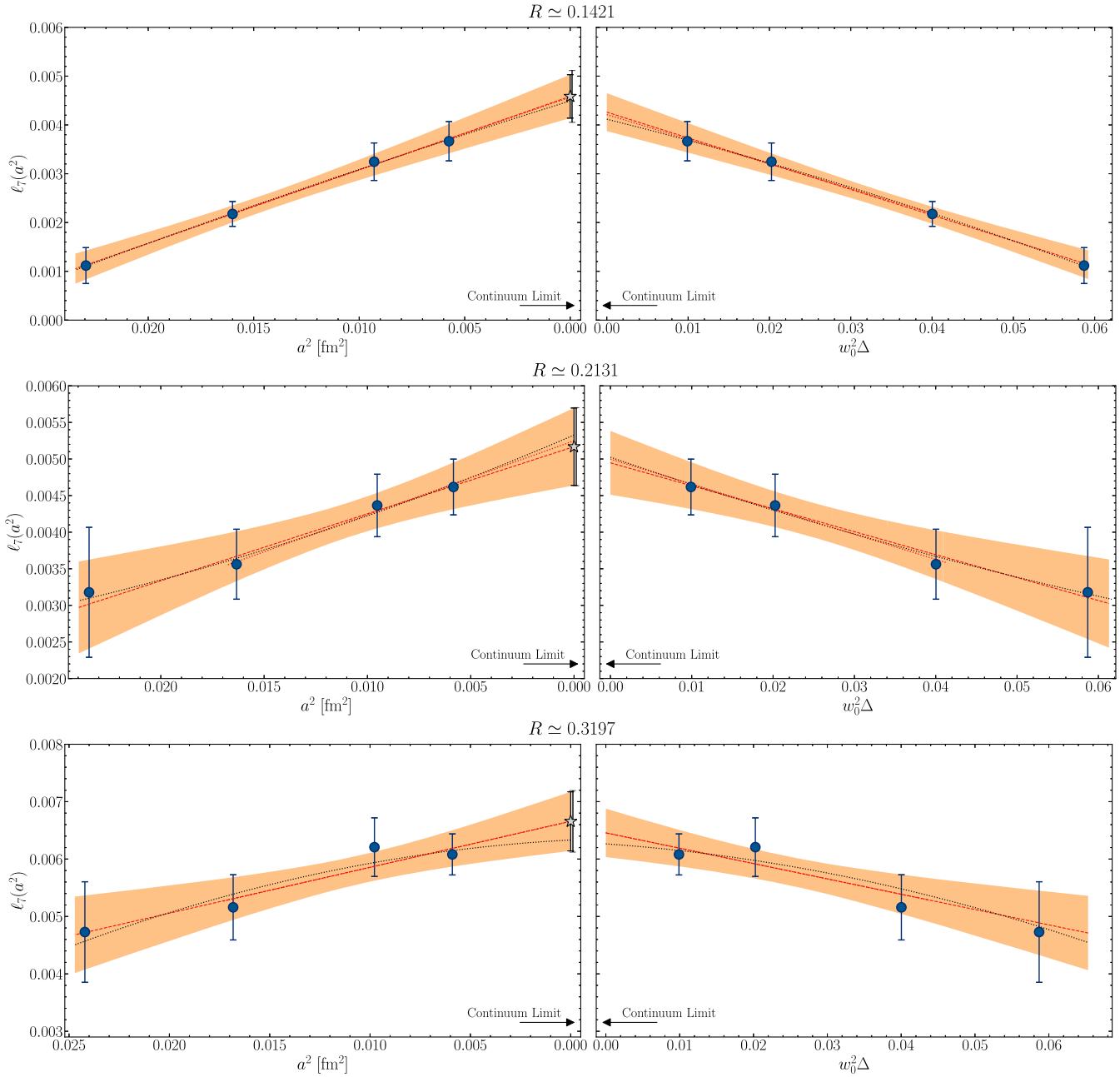

FIG. 3. Continuum limit extrapolations of ℓ_7 for the three values of the parameter $R = m_\ell/m_s^{(\mathrm{phys})}$ explored. Left panels report best fits as a function of a^2, while right panels report best fits as a function of $w_0^2\Delta$. Continuous lines (with their related continuous shaded areas) correspond to linear fits using all available data points, dashed lines represent linear fits restricted to the three finest lattice spacings, and dotted lines represent quadratic fits. The star points represent our final results for the continuum limits, and are obtained from the linear extrapolations in a^2 (no star point is represented for extrapolations in $w_0^2\Delta$, as these fits are only used to assess systematic errors). Since the total error bar, given by the sum in quadrature of the statistical and systematic uncertainties, is barely distinguishable from the statistical one for the two largest values of R, it has been slightly shifted horizontally for clarity.

structure of NNLO contributions to Eq. (1), and thus the finite quark mass corrections to Eq. (10).

The calculation of the strong pion mass splitting at NNLO in χPT is fully carried out for the first time in this study. In the following, we will report the results that are necessary for the chiral extrapolation of ℓ_7, while further details can be found in Appendix D.

Remarkably, all NNLO contributions to the pion mass splitting are $\mathcal{O}[(\Delta m)^2]$, and their structure turns out to be rather simple, as there are only two $\mathcal{O}(m_\ell)$ terms appearing

TABLE III. Continuum limits of ℓ_7 as a function of the light-to-strange quark mass ratio R. We also report the continuum limits of $M_\pi(R)$ and $F_\pi(R)$ (reported errors include both statistical and systematic uncertainties), and of the improved estimator $\tilde{\ell}_7(R)$ where leading logs have been removed via $c_1(R)$ and $c_2(R)$ (see Sec. III C for more details).

$R \equiv m_\ell/m_s^{(\mathrm{phys})}$	$\ell_7(R) \times 10^3$	$M_\pi(R)$ (MeV)	$F_\pi(R)$ (MeV)	$c_1(R)$	$c_2(R)$	$\tilde{\ell}_7(R) \times 10^3$
0.3197	$6.66(51)_{\mathrm{stat}}(15)_{\mathrm{syst}}$	384(7)	105.1(2.9)	0.637(61)	0.5541(42)	$2.37(29)_{\mathrm{stat}}(04)_{\mathrm{syst}}$
0.2131	$5.17(53)_{\mathrm{stat}}(07)_{\mathrm{syst}}$	316(6)	100.7(2.8)	0.762(52)	0.6125(37)	$2.42(27)_{\mathrm{stat}}(03)_{\mathrm{syst}}$
0.1421	$4.58(45)_{\mathrm{stat}}(29)_{\mathrm{syst}}$	265(6)	97.7(3.1)	0.857(61)	0.6715(34)	$2.64(32)_{\mathrm{stat}}(12)_{\mathrm{syst}}$

in Eq. (35). One is a chiral logarithm of order $\mathcal{O}(m_\ell \log m_\ell)$, which turns out to be proportional to ℓ_7 itself—see also [35,36], where the calculation of the leading nonanalytic contributions to ΔM_π^2, once matched to our notation, yields a chiral log multiplying ℓ_7 with the same coefficient as ours. The second is a linear $\mathcal{O}(m_\ell)$ correction, whose coefficient depends instead on some combination of the couplings of the NNLO isospin-breaking operators appearing at $\mathcal{O}(p^6)$, see Appendix D. All other corrections are higher-order in the chiral expansion, i.e., $\mathcal{O}(m_\ell^2)$ in the quark mass. In the end, Eqs. (1) and (10) are modified, respectively, as follows:

$$M_{\pi^+}^2 - M_{\pi^0}^2 = (\Delta m)^2 \frac{8B^2}{F^2} \times \left\{ \ell_7 \left[1 - 3\frac{M^2}{16\pi^2 F^2} \log\left(\frac{M^2}{16\pi^2 F^2} \right) \right] + CM^2 + \mathcal{O}(M^4) \right\}, \tag{35}$$

$$\frac{M_\pi}{M} \frac{m_\ell^2 F^2}{M^3} \frac{M_{\pi^+} - M_{\pi^0}}{(\Delta m)^2} = \ell_7 \left[1 - 3\frac{M^2}{16\pi^2 F^2} \log\left(\frac{M^2}{16\pi^2 F^2} \right) \right] + CM^2 + \mathcal{O}(M^4), \tag{36}$$

Note that, to pass from (35) to (36), we here used $\Delta M_\pi^2 \simeq 2M_\pi \Delta M_\pi$, as opposed to $\Delta M_\pi^2 \simeq 2M\Delta M_\pi$ in Eq. (9), since we are now retaining $\mathcal{O}(m_\ell)$ corrections to ℓ_7.

Inspired by Eq. (36), before performing any chiral extrapolation, we apply the following correction factors to our continuum determinations of $\ell_7(R)$ in Table III,

$$\ell_7(R) \longrightarrow \ell_7(R) \times c_1(R) \times c_2(R) \equiv \tilde{\ell}_7(R), \tag{37}$$

where the two correction factors $c_1(R)$ and $c_2(R)$ read,

$$c_1(R) = \frac{F^2}{(2Bm_s R)^2} \frac{M_\pi^4(R)}{F_\pi^2(R)}, \tag{38}$$

$$c_2^{-1}(R) = 1 - 3\frac{Bm_s R}{8\pi^2 F^2} \log\left(\frac{Bm_s R}{8\pi^2 F^2} \right). \tag{39}$$

The first factor, $c_1(R)$, takes into account the fact that, for the purpose of evaluating the prefactor of $\ell_7^{(\mathrm{eff})}$ in Eq. (23) we have used the simulated values of $M_\pi^2(R)/m_\ell$ and $F_\pi(R)$, cf. Table I, rather than their expression in the chiral limit $M^2/m_\ell = 2B$ and F, which is what actually appears in the left-hand side of Eq. (1), see [2,3,36]. This choice is irrelevant for the purpose of computing the chiral limit of $\ell_7(R)$, but of course introduces additional finite-quark-mass corrections to Eq. (36), that $c_1(R)$ aims to cancel. The second factor $c_2(R)$ aims instead to remove the $\mathcal{O}(m_\ell \log m_\ell)$ leading-log term appearing in the right-hand side of Eq. (36). To compute c_1 and c_2, we took F from the latest FLAG average, $F = 86.6(6)$ MeV [5], and $M^2/R = Bm_s = [2.36(5) \times 10^5]$ MeV^2 from [15]. For the finite-quark-mass quantities $M_\pi(R)$ and $F_\pi(R)$, instead, we took the continuum-extrapolated results of [15], reported in Table III. The correction factors and the corrected quantity $\tilde{\ell}_7$ are also found in Table III.

After the application of the two χPT-inspired corrections outlined above, we expect our corrected data for $\ell_7(R)$ to be well-described by the following function:

$$\tilde{\ell}_7(R) = \ell_7 + \tilde{C}R + \mathcal{O}(R^2), \tag{40}$$

i.e., according to a leading linear dependence in R, with no $\mathcal{O}(R \log R)$ terms, up to $\mathcal{O}(R^2)$ subleading terms. As it can be seen from Fig. 4, the corrected data show almost a flat behavior as a function of R, $\tilde{C} \simeq (-1.4 \pm 2.4) \times 10^{-3}$, and are thus in perfect agreement with our expectations. A naïve linear extrapolation in R of the uncorrected data would still give a compatible extrapolation, but with a much larger slope.

In order to propagate systematic uncertainties associated with the continuum limit to the chiral extrapolation, we followed a bootstrap-based strategy. In particular, we performed a bootstrap resampling of each data point, and added to each value of $\ell_7(R)$ a zero-mean stochastic Gaussian noise with variance equal to the squared systematic error. For each bootstrap sample we repeated the chiral fit, and estimated the final systematic error from the average absolute deviation between the central value of the chiral limits of each bootstrap sample and the central value of the chiral extrapolation obtained ignoring systematic errors. Concerning instead the systematic error related to the

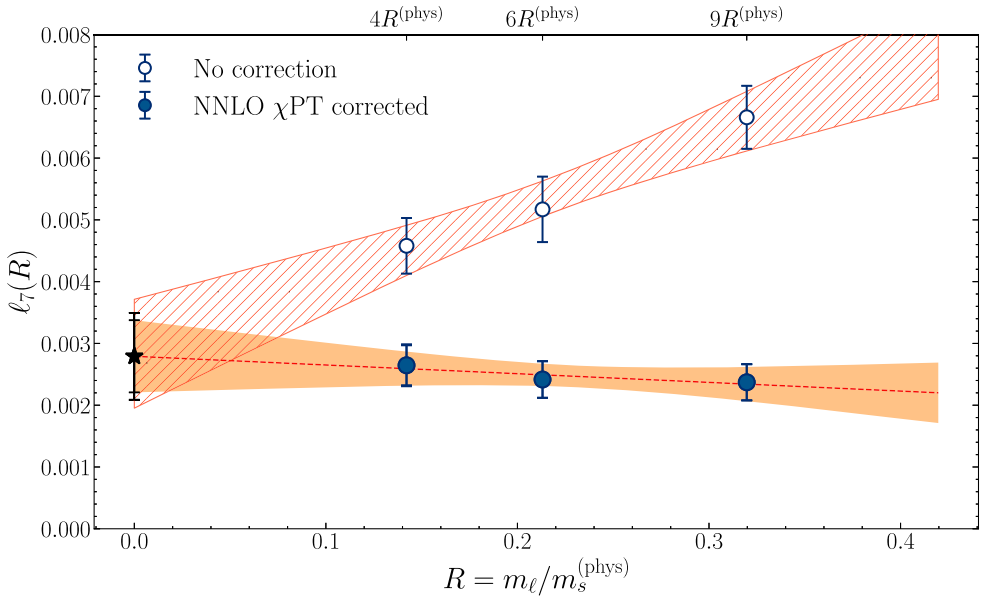

FIG. 4. Chiral limit extrapolation of the corrected values of $\ell_7(R)$ according to a linear function of the ratio $R = m_\ell/m_s^{(\mathrm{phys})}$. The full star point at $R = 0$ stands for the extrapolated value in the chiral limit, according to the best fit of the corrected data (dashed line). The two error bars plotted for the chiral extrapolation represent, respectively, the statistical and the sum of the statistical and systematic uncertainties. For the sake of comparison we also show the noncorrected data and their naive linear extrapolation, depicted as a dashed shaded band.

possible influence of higher-order $\mathcal{O}(R^2)$ terms, with only three points it is not possible to perform a comprehensive study. A possible crude estimate can however be obtained, using again Eq. (33), by comparing the linear extrapolation presented above with the one obtained from a 0-degrees-of-freedom best fit to the data corresponding to the two smallest values of R. This uncertainty is added in quadrature to the one obtained from the propagation of the systematic errors on the continuum limits.

In the end, our final result for the NLO LEC ℓ_7 in the chiral limit, including both statistical and systematic uncertainties from continuum and chiral extrapolations, and represented as a full star point in Fig. 4, reads:

$$\ell_7 \times 10^3 = 2.79(58)_{\mathrm{stat}}(19)_{\mathrm{syst}} = 2.79(61)_{\mathrm{tot}}. \qquad (41)$$

As it can be seen, our final error is dominated by statistical uncertainties (mainly due to the chiral extrapolation), which account for about the 85% of the total error budget. Therefore, further reducing it would require determinations of ℓ_7 for lower quark masses. Unfortunately, the signal-to-noise ratio of ℓ_7 rapidly deteriorates as we approach the physical point, mainly due to the disconnected contribution to ℓ_7 (see Appendix C for more details). Thus, determining ℓ_7 at, for example, the physical point $R \simeq 0.0355$ would require a very challenging numerical effort.

IV. CONCLUSIONS

In this work we presented an extensive direct lattice calculation of the QCD low-energy constant ℓ_7, which parametrizes IB effects in SU(2) χPT at NLO, adopting staggered fermions.

To this end, we employed a recently proposed method [11] to extract ℓ_7 from the strong charged/neutral pion mass splitting, based on the RM123 approach to compute derivatives with respect to the quark mass difference $\Delta m = (m_{\mathrm{d}} - m_{\mathrm{u}})/2$ from an expansion around the $\Delta m = 0$ isosymmetric theory. This method was originally proposed and applied to twisted mass Wilson fermions, and is here implemented for staggered fermions for the first time.

Our calculation utilizes three different LCPs with the same value of the strange quark mass (fixed to its physical value), and varying values of the mass of the light doublet satisfying, $M_\pi L \geq 4$. Moreover, for each LCP four values of the lattice spacing were considered. This allowed us to provide the first direct lattice determination of ℓ_7 with controlled continuum, finite-volume, and chiral extrapolations.

Our final result for this LEC in the SU(2) chiral limit, i.e., massless up and down quarks and physical-mass strange quark, is,

$$\ell_7 \times 10^3 = 2.79(58)_{\mathrm{stat}}(19)_{\mathrm{syst}} = 2.79(61)_{\mathrm{tot}}. \qquad (42)$$

A comparison with previous estimates is displayed in Fig. 5. Our result is compatible with, and significantly

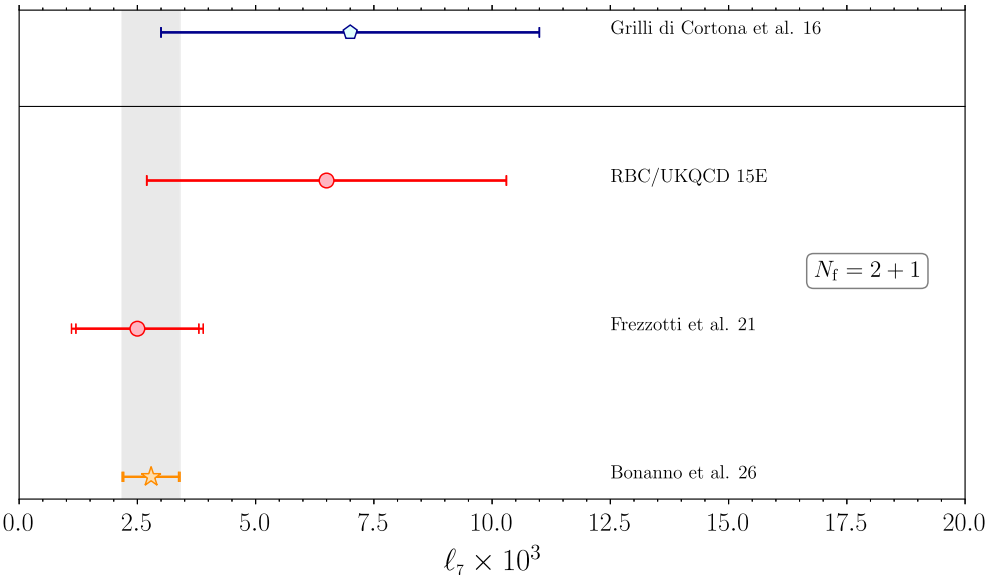

FIG. 5. Comparison of our $N_f = 2+1$ lattice determination of ℓ_7 (starred point, shaded area) with previous ones from Refs. [6,11], and with the phenomenological estimate of [4].

improves on, previous lattice determinations, $\ell_7 \times 10^3 = 6.5(3.8)_{\text{stat}}(0.20)_{\text{syst}}$ [6] (indirect determination), $\ell_7 \times 10^3 = 2.50(1.30)_{\text{stat}}(0.50)_{\text{syst}}$ [11] (direct determination for a single gauge ensemble), as well as with the phenomenological estimate $\ell_7 \times 10^3 = 7(4)$ [4].

ACKNOWLEDGMENTS

It is a pleasure to thank C. Bonati for useful discussions, and M. Gorghetto and G. Villadoro for communications about Ref. [7]. The work of C. B. is supported by the Spanish Research Agency (Agencia Estatal de Investigación) through the Grant IFT Centro de Excelencia Severo Ochoa CEX2020-001007-S and, partially, by the Grant No. PID2021-127526NB-I00, both of which are funded by MCIN/AEI/10.13039/501100011033. R. D. acknowledges funding from the European Union (EU) Next Generation EU (NGEU)—National Recovery and Resilience Plan (NRRP)—MISSION 4 COMPONENT 1, INVESTMENT N.4.1—CUP N. I51J24000160007 (PhD Cycle XL, Ministerial Decree no. 629/2024). F. S. is supported by ICSC—Centro Nazionale di Ricerca in High Performance Computing, Big Data and Quantum Computing, funded by the EU NGEU—and by the Italian Ministry of University and Research (MUR) Project No. FIS 00001556. This work has also been supported by the project "Non-perturbative aspects of fundamental interactions, in the Standard Model and beyond" funded by MUR, Progetti di Ricerca di Rilevante Interesse Nazionale (PRIN), Bando 2022, Grant No. 2022TJFCYB (CUP I53D23001440006). Numerical calculations have been performed on the Leonardo machine at Cineca, based on the agreement between INFN and Cineca, under Projects No. INF23_npqcd and No. INF24_npqcd.

DATA AVAILABILITY

The data that support the findings of this article are openly available in the tables reported in this manuscript. Further raw data are available upon reasonable request.

APPENDIX A: TASTE SYMMETRY RESTORATION IN THE CONTINUUM LIMIT OF THE PION MASS

The estimator in Eq. (23) essentially involves computing the time derivative of the difference between two four-point correlators, corresponding to the connected and disconnected diagrams in Eq. (20). A crucial step in computing these correlators is the proper choice of interpolating operators. The relevant operators are those corresponding to the neutral and charged pion, namely $\mathcal{O}_{\pi^0}$ and $\mathcal{O}_{\pi^+}$.

However, with staggered fermions there is no straightforward one-to-one correspondence between the pion fields in the continuum and those on the lattice. This problem arises due to the so-called taste symmetry [20]. Specifically, the staggered pion states are described by operators of the form $\bar{\psi}\gamma_5 \otimes \xi_S \psi$, where the taste matrices ξ_S span five irreducible representations [37],

$$\xi_S \in \{1, \xi_5, \xi_\mu, \xi_{\mu 5}, \xi_{\mu\nu}\} = \{\mathrm{I}, \mathrm{P}, \mathrm{V}, \mathrm{A}, \mathrm{T}\}, \quad \text{(A1)}$$

representing the singlet (I), pseudoscalar (P), vector (V), axial-vector (A), and tensor (T) channels. Among these, the

pseudoscalar (P) channel corresponds to the pseudo-Nambu–Goldstone boson. In the continuum limit, taste symmetry is exact, and all the staggered pions are degenerate. On the lattice, however, taste symmetry is broken at finite lattice spacing, causing the staggered pions to split into multiplets according to the tensor structure of their interpolating operators in (A1). An important consequence of taste symmetry breaking is that the order in which the continuum and chiral limits are taken becomes nontrivial. In the staggered formulation, these limits do not commute: to properly restore continuum physics, one must first take the continuum limit before performing the chiral extrapolation. This ensures the restoration of taste symmetry, leading to a degenerate pion spectrum.

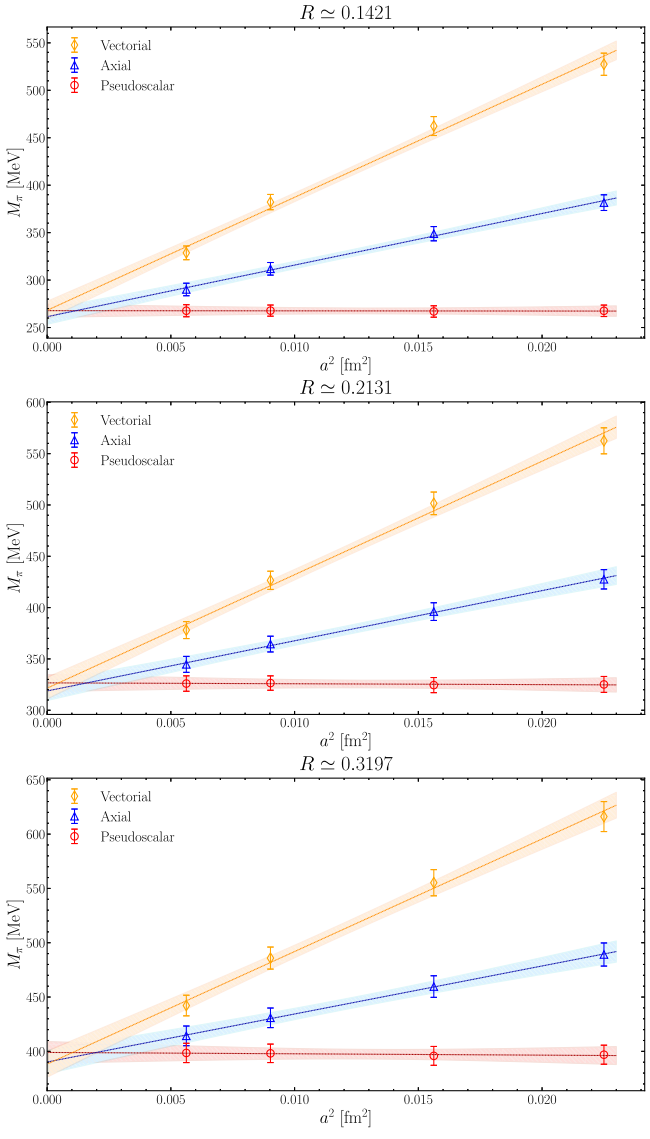

FIG. 6. Continuum limits of the pion masses extracted from interpolating operators with different taste structure for all the gauge ensembles employed in this study.

At finite lattice spacing, however, if the chiral limit is taken first, only the mass of the pion associated with the pseudoscalar channel vanishes. This behavior is due to the fact that staggered fermions preserve a remnant of the chiral symmetry of the continuum theory, protecting the pseudo-Nambu–Goldstone boson from acquiring a mass. Hence, a controlled continuum extrapolation is essential to recover the full taste symmetry structure and the correct physical pion spectrum [37]. As shown in Fig. 6, we have indeed verified with our data that this is the case.

APPENDIX B: COMPARISON OF ℓ_7 DETERMINATIONS FROM THE PSEUDOSCALAR, VECTOR AND AXIAL-VECTOR CHANNELS

As outlined in Sec. III, no signal was obtained for the disconnected contribution in the customary pseudoscalar channel, motivating our choice of using the axial channel throughout the calculations presented in this study. In this appendix we show, in Fig. 7, the improvement in the signal

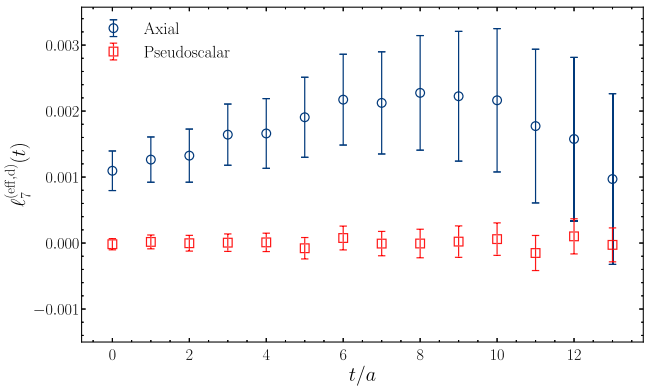

FIG. 7. Comparison of the disconnected contribution to ℓ_7 obtained from the pseudoscalar and the axial channels, for $a \simeq 0.0964$ fm and $R \simeq 0.1421$.

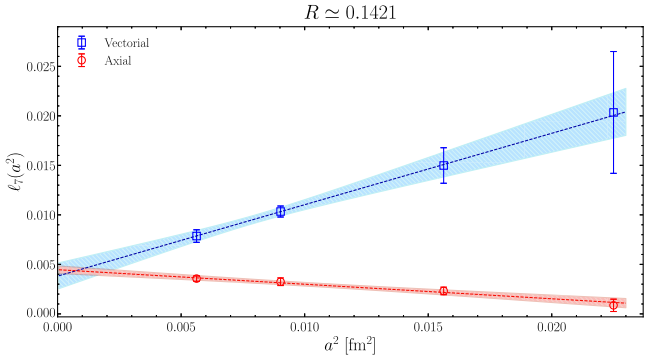

FIG. 8. Comparison of our determinations of ℓ_7 from the vector and the axial-vector channels for $R \simeq 0.1421$.

for the disconnected contribution $\ell_7^{(\mathrm{eff,d})}$ obtained using the axial channel with respect to the pseudoscalar one.

As a further check of our procedure, we also extracted ℓ_7 using Eq. (23) from the vector channel. Despite results differing from the axial-vector ones at finite lattice spacing, the two determinations nicely converge toward the same continuum limit, see Fig. 8. This is not surprising, giving that all interpolating operators, in the continuum limit, describe exactly the same particle with the same mass, cf. also Appendix A. Since the axial-vector channel gave smaller uncertainties with respect to the vector one, we chose the former to perform our final calculations.

APPENDIX C: SCALING OF THE SIGNAL-TO-NOISE RATIO OF ℓ_7 TOWARD THE CHIRAL LIMIT

Our final result for ℓ_7 is dominated by statistical uncertainties due to the chiral extrapolation. Thus, improving our final error would require to perform direct determinations of ℓ_7 for lower values of m_ℓ. However, we observed a rapid deterioration of the signal-to-noise ratio of this quantity when approaching the chiral limit.

In order to quantify this effect, we studied the scaling of the statistical variance of $\ell_7^{(\mathrm{eff})}(t)$ as a function of the quark mass for a fixed time slice in the region where the plateau is observed. For each mass, we considered the finest available lattice spacing $a \simeq 0.075$ fm, and computed the variance of $\ell_7^{(\mathrm{eff})}$—both for the full estimator and for its connected and disconnected components—multiplied by the total number of configurations of the corresponding ensemble. This rescaling allowed us to isolate the intrinsic noise of our observable of choice in a statistics-independent way. The results, shown in Fig. 9, display a clear rapid growth of the rescaled variance as the chiral limit is approached.

Furthermore, as shown in the main text (see Sec. III), the signal for ℓ_7 tends to decrease linearly with the quark mass toward the chiral limit. The combination of a diminishing signal and of rapidly growing statistical fluctuations makes a reliable determination of ℓ_7 at, say, the physical point, currently unfeasible with the typical statistics that can be generated with an affordable numerical effort.

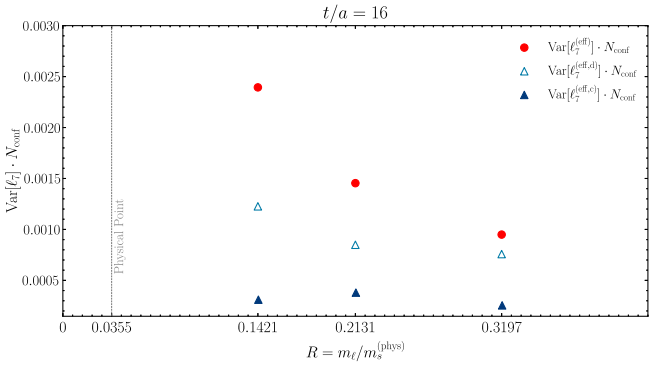

FIG. 9. Scaling of the rescaled variance of $\ell_7^{(\mathrm{eff})}(t)$ (and its connected/disconnected components) for a time slice in the plateau region ($t/a = 16$) as a function of $R = m_\ell/m_s^{(\mathrm{phys})}$ for the finest lattice spacing of each LCP considered in this study.

APPENDIX D: CHARGED AND NEUTRAL PION MASSES AT NNLO IN χPT

At NNLO in the chiral expansion, the charged and neutral pion masses can be written as follows:

$$M_{\pi^+}^2 = M^2(1 + m_1 + m_2), \tag{D1}$$

$$\Delta M_\pi^2 = M^2\Delta^2(\delta_1 + \delta_2), \tag{D2}$$

with $\Delta M_\pi^2 = M_{\pi^+}^2 - M_{\pi^0}^2$ the strong pion mass splitting. In these formulas, $M^2 = 2Bm_\ell$, $\Delta \equiv \Delta m_\ell/m_\ell$, while m_1, δ_1 and m_2, δ_2 are, respectively, the NLO and NNLO χPT corrections for the charged pion mass and the pion mass splitting. Their explicit expressions read,

$$m_1 = 2\frac{M^2}{F^2}[\ell_3^r(\mu) + L(\mu)], \tag{D3}$$

$$\begin{aligned} m_2 = \frac{M^4}{F^4}\Bigg\{ & \frac{17}{8}L^2(\mu) - 16C_2(\mu) \\ & - \left[(14\ell_1^r + 8\ell_2^r + 3\ell_3^r)(\mu) + \frac{49}{192\pi^2}\right]L(\mu) \\ & + \frac{1}{16\pi^2}(\ell_1^r + 2\ell_2^r + l_3^r)(\mu) + \frac{163}{96}\frac{1}{(16\pi^2)^2} \\ & - \Delta^2[\ell_7 L(\mu) + 16C_2'(\mu)]\Bigg\}, \end{aligned} \tag{D4}$$

$$\delta_1 = 2\frac{M^2}{F^2}\ell_7, \tag{D5}$$

$$\delta_2 = 2\frac{M^4}{F^4}\left[-3\ell_7 L(\mu) + 16C_{\mathrm{IB}}(\mu) - \frac{\ell_7}{32\pi^2}\right]. \tag{D6}$$

In Eqs. (D3)–(D6), we have used the following shorthands:

$$L(\mu) \equiv \frac{1}{16\pi^2}\log\left(\frac{M^2}{\mu^2}\right) \tag{D7}$$

is the chiral log, while

$$\begin{aligned} C_2 \equiv\ & 2c_6^r + c_7^r + 2c_8^r + c_9^r \\ & - 3c_{10}^r - 6c_{11}^r - 2c_{17}^r - 4c_{18}^r, \end{aligned} \tag{D8}$$

$$C_2' \equiv c_7^r - c_9^r - 3c_{10}^r - 2c_{11}^r, \tag{D9}$$

$$C_{\mathrm{IB}} \equiv c_9^r - 3c_{10} - 2c_{11}^r - 3c_{17}^r - 2c_{18}^r - 4c_{19}^r, \tag{D10}$$

indicate specific combinations of the 57 renormalized LECs c_i^r appearing in the two-flavor chiral Lagrangian in χPT at NNLO.

The expressions for m_1 and δ_1 date back to Gasser and Leutwyler [2,3,36], while the expression for m_2 was previously computed in Refs. [38,39] only in the isospin-symmetric case $\Delta = 0$, and neglecting the contributions coming from the NNLO LECs, as these were only introduced later [34,40]. Thus, the full expression of m_2 (including isospin-breaking corrections and the NNLO LECs contributions) and of δ_2 are new results first presented in this study. Note also that our NNLO formula for $M_{\pi^0}^2$ corrects a misprint in Eq. (A6) of Ref. [7].[4]

Coming back to ΔM_π^2, the running of $C_{\rm IB}(\mu)$ and $L(\mu)$ is such that δ_2 is renormalization-group invariant. Thus, one may also rewrite the NNLO correction to the strong pion mass splitting as,

$$\delta_2 = -6\ell_7 \frac{M^4}{16\pi^2 F^4} \log\left(\frac{M^2}{\Lambda_{\rm IB}^2}\right), \tag{D11}$$

with

$$\Lambda_{\rm IB} \equiv \mu \exp\left\{\frac{128\pi^2}{3}\frac{C_{\rm IB}(\mu)}{\ell_7} - \frac{1}{12}\right\} \tag{D12}$$

a physical (i.e., μ independent) energy scale characterizing isospin breaking at NNLO.

Adopting the representation for δ_2 in Eq. (D6), setting

$$\mu = \mu_0 \equiv 4\pi F = 1.088(8)\ \text{GeV}, \tag{D13}$$

and substituting

$$C \equiv 16\frac{C_{\rm IB}(\mu_0)}{F^2} - \frac{\ell_7}{32\pi^2 F^2}, \tag{D14}$$

one easily obtains Eq. (35) in the main text. From the chiral fit of the corrected data $\widetilde{\ell}_7(R)$, we instead extracted the quantity $\tilde{C}$, cf. Eq. (40), which is related to $C_{\rm IB}(\mu_0)$ via the following relation:

$$\tilde{C} = 2\frac{Bm_{\rm s}}{F^2}\left[16C_{\rm IB}(\mu_0) - \frac{\ell_7}{32\pi^2}\right]. \tag{D15}$$

Since we found, from the chiral fit,

$$\tilde{C} = (-1.4 \pm 2.4) \times 10^{-3}, \tag{D16}$$

we obtain,

$$C_{\rm IB}(\mu_0) = (-8 \pm 24) \times 10^{-7}. \tag{D17}$$

This value for $C_{\rm IB}(\mu_0)$ implies,

$$\frac{\Lambda_{\rm IB}}{\mu_0} = \frac{\Lambda_{\rm IB}}{4\pi F} = 0.87(32), \tag{D18}$$

$$\Rightarrow \Lambda_{\rm IB} \simeq 0.95(35)\ \text{GeV}. \tag{D19}$$

APPENDIX E: DETERMINATION OF $\bar{\ell}_3$ AND $\bar{\ell}_4$

The determinations of M_π and F_π reported in the present study in Table III, and used for the calculation of ℓ_7, can also be employed to extract two other NLO LECs: $\bar{\ell}_3$ and $\bar{\ell}_4$. These couplings parametrize the corrections to the chiral limits of the pion mass and of the pion decay constant [3],

$$M_\pi^2 = M^2\left\{1 - \frac{M^2}{32\pi^2 F^2}[\bar{\ell}_3 - L(M)]\right\}, \tag{E1}$$

$$F_\pi = F\left\{1 + \frac{M^2}{16\pi^2 F^2}[\bar{\ell}_4 - L(M)]\right\}, \tag{E2}$$

with

$$L(M) = \log\left(\frac{M^2}{M_\pi^{(\rm phys)2}}\right), \tag{E3}$$

$$M_\pi^{(\rm phys)} = 135\ \text{MeV}, \tag{E4}$$

a chiral log. Using $M^2 = 2Bm_\ell = 2Bm_{\rm s}R$, one can perform a four-parameter global fit of $M_\pi(R)$ and $F_\pi(R)$ and extract $\bar{\ell}_3$ and $\bar{\ell}_4$,

$$\frac{M_\pi^2(R)}{R} = 2Bm_{\rm s}\left\{1 - \frac{Bm_{\rm s}R}{16\pi^2 F^2}[\bar{\ell}_3 - \tilde{L}(R)]\right\}, \tag{E5}$$

$$F_\pi(R) = F\left\{1 + \frac{Bm_{\rm s}R}{8\pi^2 F^2}[\bar{\ell}_4 - \tilde{L}(R)]\right\}, \tag{E6}$$

where now the chiral log reads

$$\tilde{L}(R) = \log\left(\frac{2Bm_{\rm s}R}{M_\pi^{(\rm phys)2}}\right). \tag{E7}$$

The joint fit was performed after the application of the finite-volume corrections R_{M_π} and R_{F_π} (cf. Sec. III B), which turned out to be always smaller than our statistical uncertainties.

The LO LECs $\Sigma m_{\rm s} = Bm_{\rm s} \times F^2$ and F were already given in the original paper [15], while $\bar{\ell}_3$ and $\bar{\ell}_4$ are reported here for the first time. We find,

[4] As confirmed by the authors of [7] via private communication.

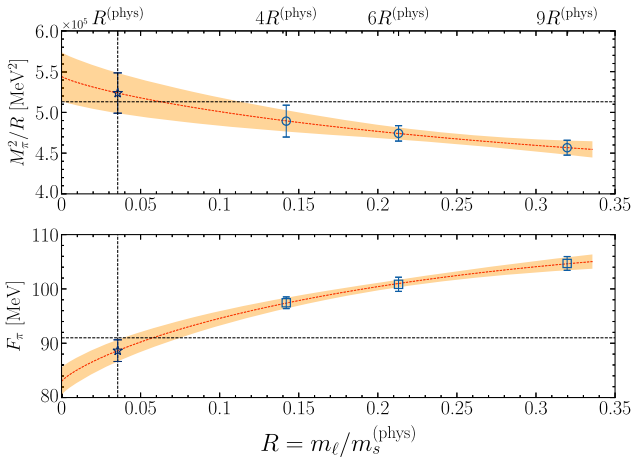

FIG. 10. Joint chiral fit of the determinations of $M_\pi(R)$ and $F_\pi(R)$ of Table I as a function of the quark mass ratio $R = m_\ell/m_s^{(\mathrm{phys})}$ according to NLO χPT predictions in Eqs. (E5) and (E6). Dashed lines represent the physical point $R \simeq 0.036$ [5] and the physical values of M_π and F_π. Starred points represent our extrapolations in $R = R^{(\mathrm{phys})}$.

$$\bar{\ell}_3 = 4.18(60)_{\mathrm{stat}}(70)_{\mathrm{syst}} = 4.18(92)_{\mathrm{tot}}, \tag{E8}$$

$$\bar{\ell}_4 = 3.90(20)_{\mathrm{stat}}(27)_{\mathrm{syst}} = 3.90(34)_{\mathrm{tot}}. \tag{E9}$$

The analysis for $\bar{\ell}_3$ and $\bar{\ell}_4$ goes along the same lines of the one for ℓ_7 presented in the main text. The central values and the statistical uncertainties are obtained from the joint chiral fit including all available points, shown in Fig. 10. The systematic error is the result of the quadrature sum of two error sources. One is the propagation of the systematic uncertainties on F_π and M_π due to the continuum extrapolation. The other is the observed difference in the fit results for $\bar{\ell}_3$ and $\bar{\ell}_4$ when including/excluding the point at the heaviest pion mass from the joint chiral fit.

Our chiral extrapolations of F_π and M_π are well under control, as it can be seen by the very good agreement of our results in $R = R^{(\mathrm{phys})} \simeq 0.036$ [5] with the physical values $M_\pi^{(\mathrm{phys})} = 135$ MeV and $F_\pi^{(\mathrm{phys})} = 92$ MeV. Moreover, our results for $\bar{\ell}_3$ and $\bar{\ell}_4$ are in very good agreement both with the latest FLAG world averages [5] and with previous determinations in the literature. This comparison is illustrated in Fig. 11.

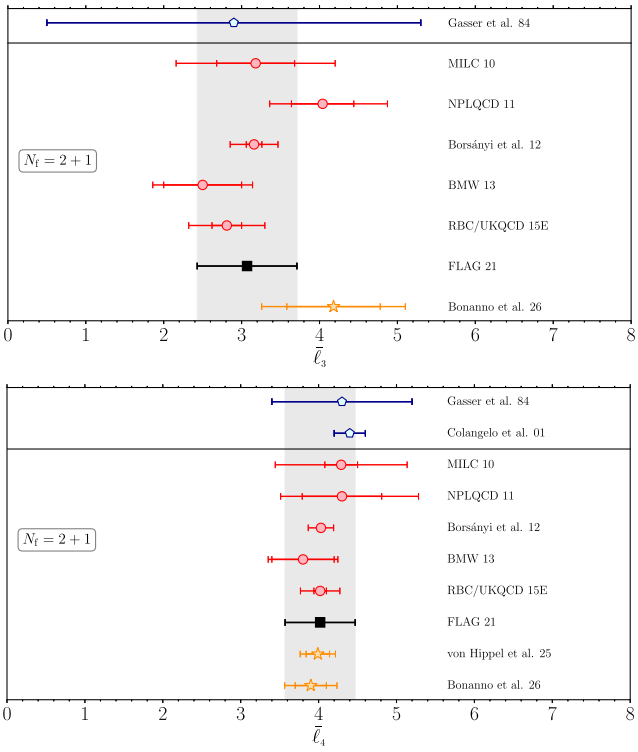

FIG. 11. Comparison of our $N_f = 2+1$ lattice determinations of $\bar{\ell}_3$ (top panel) and $\bar{\ell}_4$ (bottom panel), drawn as starred points, with previous ones [6,41–44] entering FLAG 21 averages [5] (square points and shaded bands). For $\bar{\ell}_4$ we also reported the recent determination of [45,46]. We also show the phenomenological estimates of [2,47].

[1] J. Goldstone, A. Salam, and S. Weinberg, Phys. Rev. **127**, 965 (1962).
[2] J. Gasser and H. Leutwyler, Ann. Phys. (N.Y.) **158**, 142 (1984).
[3] J. Gasser and H. Leutwyler, Nucl. Phys. **B250**, 465 (1985).
[4] G. Grilli di Cortona, E. Hardy, J. Pardo Vega, and G. Villadoro, J. High Energy Phys. 01 (2016) 034.
[5] Y. Aoki *et al.* (Flavour Lattice Averaging Group (FLAG) Collaboration), Eur. Phys. J. C **82**, 869 (2022).
[6] P. A. Boyle *et al.*, Phys. Rev. D **93**, 054502 (2016).
[7] M. Gorghetto and G. Villadoro, J. High Energy Phys. 03 (2019) 033.
[8] L. Di Luzio, G. Martinelli, and G. Piazza, Phys. Rev. Lett. **126**, 241801 (2021).
[9] L. Di Luzio, J. Martin Camalich, G. Martinelli, J. A. Oller, and G. Piazza, Phys. Rev. D **108**, 035025 (2023).
[10] L. Di Luzio and G. Piazza, J. High Energy Phys. 12 (2022) 041; 05 (2023) 018.

[11] R. Frezzotti, G. Gagliardi, V. Lubicz, G. Martinelli, F. Sanfilippo, and S. Simula, Phys. Rev. D **104**, 074513 (2021).
[12] G. M. de Divitiis *et al.*, J. High Energy Phys. 04 (2012) 124.
[13] D. Giusti, V. Lubicz, C. Tarantino, G. Martinelli, F. Sanfilippo, S. Simula, and N. Tantalo, Phys. Rev. D **95**, 114504 (2017).
[14] R. Frezzotti, G. Gagliardi, V. Lubicz, F. Sanfilippo, and S. Simula, Eur. Phys. J. A **57**, 282 (2021).
[15] C. Bonanno, F. D'Angelo, and M. D'Elia, J. High Energy Phys. 11 (2023) 013.
[16] C. Morningstar and M. J. Peardon, Phys. Rev. D **69**, 054501 (2004).
[17] M. A. Clark and A. D. Kennedy, Phys. Rev. D **75**, 011502 (2007).
[18] M. A. Clark and A. D. Kennedy, Phys. Rev. Lett. **98**, 051601 (2007).
[19] Y. Aoki, S. Borsányi, S. Dürr, Z. Fodor, S. D. Katz, S. Krieg, and K. K. Szabo, J. High Energy Phys. 06 (2009) 088.
[20] S. Borsányi, G. Endrődi, Z. Fodor, A. Jakovac, S. D. Katz, S. Krieg, C. Ratti, and K. K. Szabo, J. High Energy Phys. 11 (2010) 077.
[21] S. Borsányi, Z. Fodor, C. Hoelbling, S. D. Katz, S. Krieg, and K. K. Szabo, Phys. Lett. B **730**, 99 (2014).
[22] S. Borsányi, S. Dürr, Z. Fodor, C. Hoelbling, S. D. Katz, S. Krieg, T. Kurth, L. Lellouch, T. Lippert, and C. McNeile (BMW Collaboration), J. High Energy Phys. 09 (2012) 010.
[23] G. S. Bali, F. Bruckmann, M. Constantinou, M. Costa, G. Endrődi, S. D. Katz, H. Panagopoulos, and A. Schafer, Proc. Sci. LATTICE2013 (**2014**) 187.
[24] M. F. L. Golterman and J. Smit, Nucl. Phys. **B255**, 328 (1985).
[25] N. Ishizuka, M. Fukugita, H. Mino, M. Okawa, and A. Ukawa, Nucl. Phys. **B411**, 875 (1994).
[26] C. Aubin and C. Bernard, Phys. Rev. D **76**, 014002 (2007).
[27] G. Colangelo and C. Haefeli, Phys. Lett. B **590**, 258 (2004).
[28] G. Colangelo, S. Dürr, and C. Haefeli, Nucl. Phys. **B721**, 136 (2005).
[29] G. Colangelo and C. Haefeli, Nucl. Phys. **B744**, 14 (2006).
[30] N. Husung, P. Marquard, and R. Sommer, Eur. Phys. J. C **80**, 200 (2020).
[31] N. Husung, arXiv:2501.17036.
[32] A. Boccaletti *et al.*, arXiv:2407.10913.
[33] C. Alexandrou *et al.* (Extended Twisted Mass Collaboration (ETMC) Collaboration), Phys. Rev. Lett. **130**, 241901 (2023).
[34] J. Bijnens, G. Colangelo, and G. Ecker, Ann. Phys. (N.Y.) **280**, 100 (2000).
[35] J. Gasser, Ann. Phys. (N.Y.) **136**, 62 (1981).
[36] J. Gasser and H. Leutwyler, Phys. Rep. **87**, 77 (1982).
[37] C. Bernard *et al.*, Proc. Sci., LATTICE2007 (**2007**) 310 [arXiv:0710.3124].
[38] U. Bürgi, Nucl. Phys. **B479**, 392 (1996).
[39] J. Bijnens, G. Colangelo, G. Ecker, J. Gasser, and M. E. Sainio, Nucl. Phys. **B508**, 263 (1997); **B517**, 639(E) (1998).
[40] J. Bijnens, G. Colangelo, and G. Ecker, J. High Energy Phys. 02 (1999) 020.
[41] A. Bazavov *et al.* (MILC Collaboration), Proc. Sci., LATTICE2010 (**2010**) 074 [arXiv:1012.0868].
[42] S. R. Beane, W. Detmold, P. M. Junnarkar, T. C. Luu, K. Orginos, A. Parreno, M. J. Savage, A. Torok, and A. Walker-Loud, Phys. Rev. D **86**, 094509 (2012).
[43] S. Borsányi, S. Durr, Z. Fodor, S. Krieg, A. Schafer, E. E. Scholz, and K. K. Szabo, Phys. Rev. D **88**, 014513 (2013).
[44] S. Dürr *et al.* (BMW Collaboration), Phys. Rev. D **90**, 114504 (2014).
[45] G. von Hippel and K. Ottnad, Phys. Rev. Lett. **135**, 071904 (2025).
[46] K. Ottnad and G. von Hippel, Phys. Rev. D **112**, 034504 (2025).
[47] G. Colangelo, J. Gasser, and H. Leutwyler, Nucl. Phys. **B603**, 125 (2001).